Supplementary information for:
Large scale InSAR monitoring of permafrost freeze-thaw cycles on the Tibetan Plateau

Simon Daout,[1*] Marie-Pierre Doin,[1], Anne Socquet[1], Cécile Lasserre[1]

[1] Universit Grenoble Alpes, CNRS, ISTerre, F-38000 Grenoble
[2]Department of Earth Science, University of California, LA, USA

Methods

This method section provides additional text and figures explaining and illustrating all the processing steps of the SAR data. We take as example the Envisat track 119, but applied the same processing scheme for all tracks.

Interferogram network. For the four tracks we first define an optimal small baseline interferometric network connecting with redundancy all acquisitions using perpendicular baseline constraint, B_{perp}, and temporal baseline constraint, B_t (Fig. S1). Note that some interferograms present either large B_{perp} and low B_t or low B_{perp} and large B_t.

Corrections before phase unwrapping. The processing is based on a series of corrections before unwrapping that reduces the variance of the wrapped phase. Fig. S2 presents an example of a long temporal baseline wrapped interferogram on track 119 before and after this series of corrections, which includes the stratified atmospheric delay correction using global atmospheric re-analysis model, ERA-Interim (1; 2; 3) (computed by the European Center for Medium-Range Weather Forecast (ECMWF)), the range ramp correction, and local Digital Elevation Model (DEM) error correction.

Unwrapping procedure. First, we perform a Principal Component Analysis (PCA) decomposition from a selection of successfully unwrapped interferograms, $\mathcal{C} = \mathcal{U} * \lambda * \mathcal{V}$, where $\mathcal{U}$ is the eigenvector matrix of the covariance matrix, $\mathcal{C}$, between interferograms centered around the zero phase, λ, is the eigenvalue matrix, and $\mathcal{V}$, is the transformation matrix from the interferograms basis to the principal component basis. $\mathcal{C}$ is computed using only unwrapped pixels. As the no data mask is slightly different from one interferograms to the other, $\mathcal{C}$ is not perfectly positive definite. The deformation pattern we are interested in pops up in the first or second component (Fig. S3a). Temporal inversion of the corresponding eigenvector shows, as expected, a seasonal signal.

The comparison of the deformation pattern extracted from PCA with elevation and google earth imagery shows that deformation is concentrated in basins and that "basement" can be considered, on average, as non deforming. We must thus insure that the deformation template extracted from PCA map is on average referenced to zero on basement. To do so, we extract a N-S profile (Fig. S3b) and observe that PCA values on basement pixels have far less scatter than the PCA values on basin pixels. To define a N-S reference curve, we fit across the median of pixels selected in areas with less scatter (red median) a cubic ramp in azimuth (blue line in Fig. S3b). This ramp in azimuth is removed from the PCA as shown in Fig. S3c.

We repeat the operation for the four tracks and observe a good spatial continuity of the extracted deformation shape on the overlapping areas that correlates with the low elevation basins (Fig. S4).

Then, following (4), we use the PCA map as a deformation template to help unwrapping in high fringe rate areas. We estimate a best-fit correlation coefficient between the deformation template and the wrapped phase (by maximizing the complex coherence of the residue), and remove the scaled template from the original interferogram (Fig. S5). Before corrections (a,b), black arrows point out typical patterns of deformation dominating the wrapped phase. After correction, these patterns are in majority removed (c) and the phase is more easily unwrapped (d).

Unwrapping process is finally performed using a specific scheme and an iterative procedure. First, we multilook by a factor of 8 in range and 40 in azimuth, replacing the amplitude of the interferograms by the colinearity as defined by (5) (Fig. S5a). We then low pass filter using the average temporal coherence extracted from the DEM correction as weight (Fig. S5b). In contrast to the cut-tree algorithm (6), here we impose an unwrapping path going from the high to low coherence areas defined by the filter, avoiding unwrapping to propagate into incoherent areas, as snow-capped mountain ridges, sand covered deserts or across areas of very high rate. Unwrapping is performed in adjoining sub-regions above a coherence threshold. Each newly unwrapped area is added to already unwrapped areas. The coherence threshold progressively slightly decreases to propagate unwrapping further away (7; 8; 9). If necessary, high priority bridges are set manually by visual inspection of interferograms.

We finally reintroduce the scaled template previously removed (e). Doing so, we successfully produce wide, continuous and high quality unwrapped interferograms covering the northwestern part of the Tibetan plateau.

Time series analysis At the end of the processing, interferograms are inverted into successive phase delays maps (Fig. 6). This step is crucial as it allows to check the consistency of each interferogram and thus detect the residual unwrapping errors (4; 10). Misclosure of the interferometric network are computed for each interferogram. If large, we then check visually the corresponding interferogram and correct its unwrapping errors. Times series analysis is then iterated again until no large network inconsistencies remain (8). To refer the maps to a stable bedrock, we first mask the deformation areas using a threshold on the previous deformation shape extracted from the PCA (Fig. S4), and estimate a cubic ramp in azimuth and a quadratic ramp in range on bedrock areas. After correction of this large scale reference surface, we derive a linear term, V, a DEM error coefficient, α, a cosinus term, β_2, and a sinus term, β_1, such as:

$$\phi^k = Vt_k + \alpha B_\perp^k + \beta_1 * \sin wt_k + \beta_2 * \cos wt_k, \quad (1)$$

and produce continuous amplitude ($\sqrt{\beta_1^2 + \beta_2^2}$), temporal lag ($\arctan \frac{\beta_1}{\beta_2}$) and ground velocity ($V$) deformation maps (Fig. 6). Model and residual maps are also shown in Fig. 6. Note that here no temporal smoothing have been applied to ϕ^k.

References

[1] Dee, D. *et al.* The ERA-Interim reanalysis: Configuration and performance of the data assimilation system. *Quarterly J. the Royal Meteorological Society* **137**, 553–597 (2011).

[2] Doin, M.-P., Lasserre, C., Peltzer, G., Cavalié, O. & Doubre, C. Corrections of stratified tropospheric delays in SAR interferometriy: Validation with global atmospheric models. *J. Applied Geophysics* **69**, 35–50 (2009).

[3] Jolivet, R., Grandin, R., Lasserre, C., Doin, M.-P. & Peltzer, G. Systematic InSAR tropospheric phase delay corrections from global meteorological reanalysis data. *Geophys. Res. Lett.* **38** (2011).

[4] López-Quiroz, P., Doin, M.-P., Tupin, F., Briole, P. & Nicolas, J.-M. Time series analysis of Mexico City subsidence constrained by radar interferometry. *J. Applied Geophysics* **69**, 1–15 (2009).

[5] Pinel-Puyssegur, B., Michel, R. & Avouac, J.-P. Multi-Link InSAR Time Series: Enhancement of a Wrapped Interferometric Database. *IEEE J. Selected Topics in Applied Earth Observations and Remote Sensing* **5**, 784–794 (2012).

[6] Rosen, P. A., Hensley, S., Peltzer, G. & Simons, M. Updated repeat orbit interferometry package released. *Eos, Transactions American Geophysical Union* **85**, 47–47 (2004).

[7] Grandin, R. *et al.* Long-term growth of the Himalaya inferred from interseismic InSAR measurement. *Geology* **40**, 1059–1062 (2012).

[8] Doin, M.-P. *et al.* InSAR measurement of the deformation around Siling Co Lake: Inferences on the lower crust viscosity in central Tibet. *J. Geophys. Res.: Solid Earth* **120**, 5290–5310 (2015).

[9] Daout, S. *et al.* Along-strike variations of the partitioning of convergence across the Haiyuan fault system detected by InSAR. *GJI* **205**, 536–547 (2016).

[10] Doin, M.-P. *et al.* Presentation of the small baseline NSBAS Processing chain on a case example : The etna deformation monitoring from 2003 to 2010 using Envisat data. *Proc. ESA Fringe* (2011).

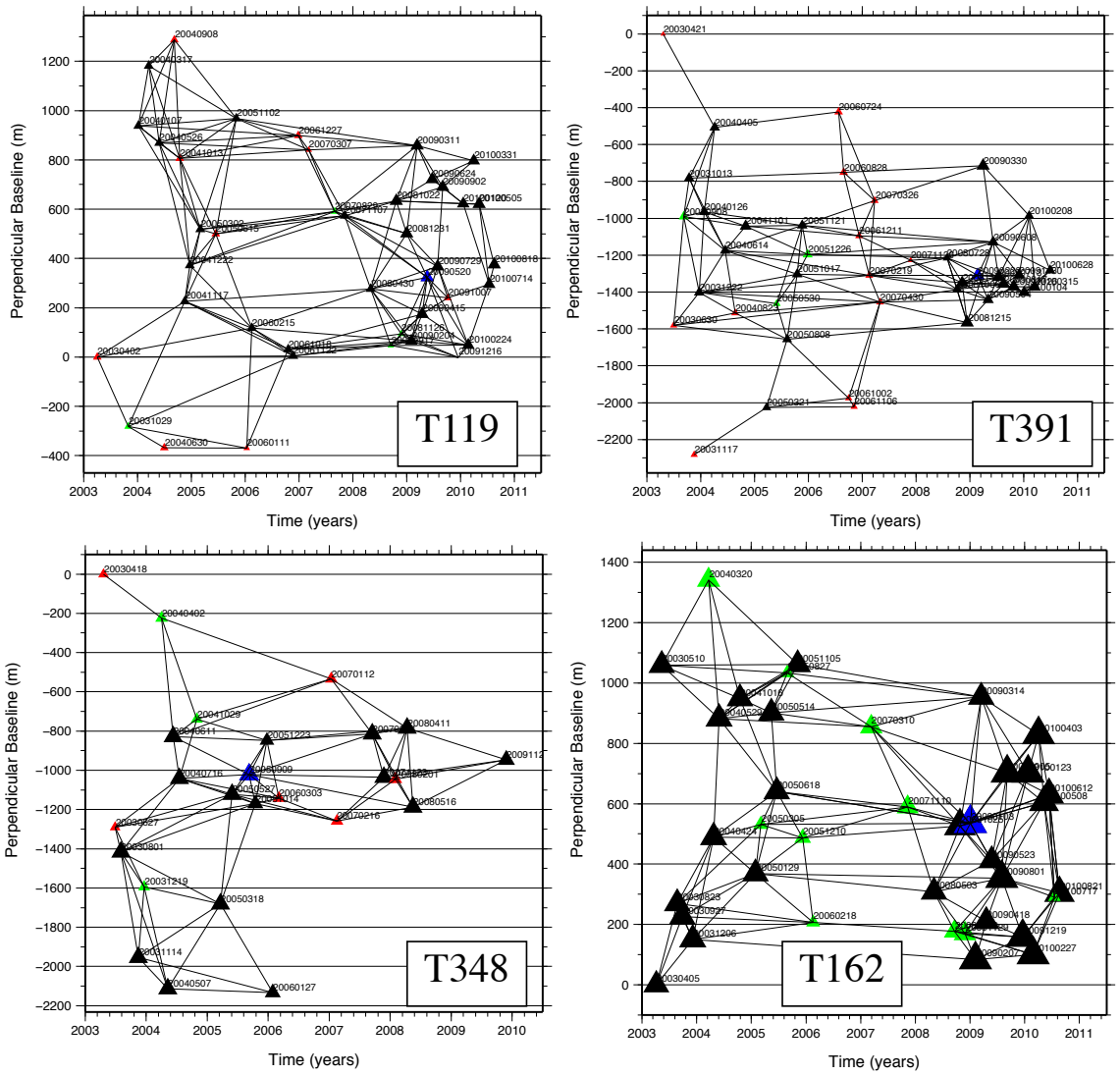

Figure S1: Computed interferograms for the four tracks. Triangles are SAR acquisitions with sizes and colors according to their spatial extent: black triangles for a full coverage, green triangles for images covering the northern part of the track only, and red colors for images covering the southern part only. The master image is shown with a blue triangle.

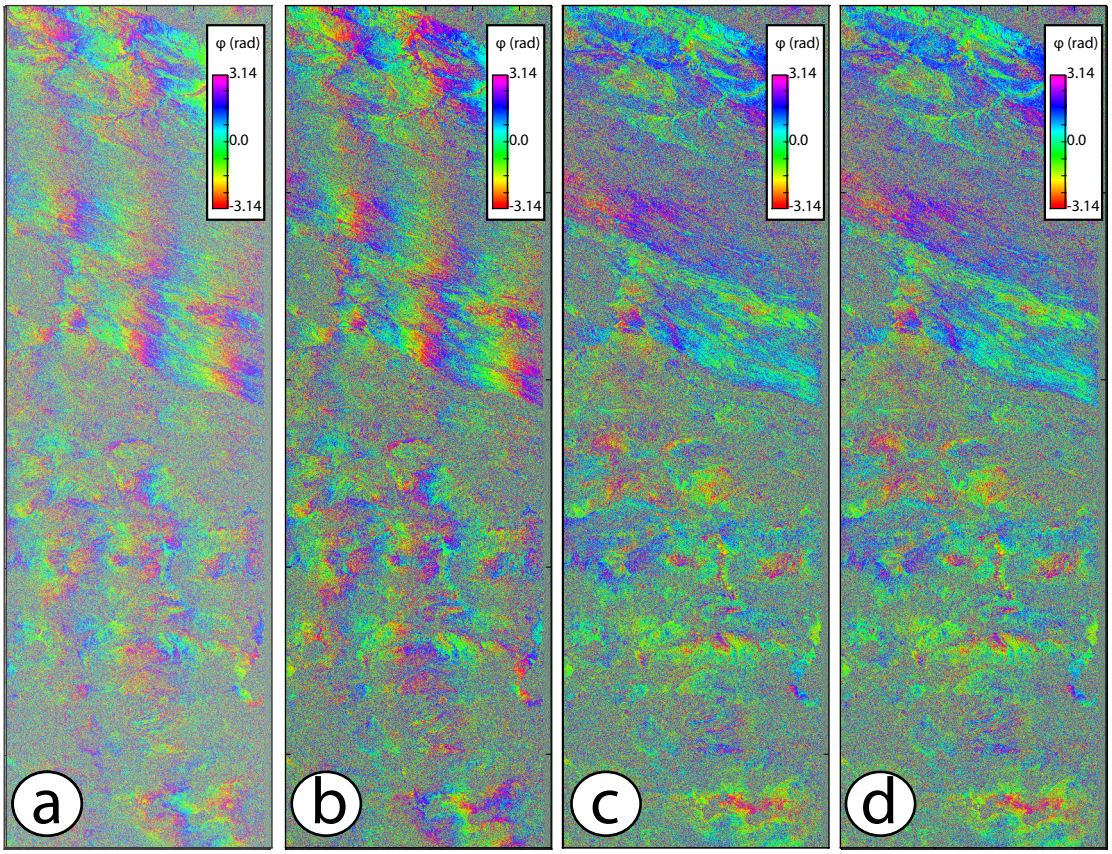

Figure S2: Example of corrections on the wrapped phase for a small B_{perp} of 50 m and long temporal baseline interferogram between the two images acquired in November 17, 2004 and April 30, 2008 for track 119. a) Original interferogram in 4x20 looks. b) Interferogram after ERAI correction. c) Interferogram after range ramp correction. d) Interferogram after local DEM errors correction. (a), (b) and (c) are superimposed to the coherence, while (d) is superimposed to the phase colinearity.

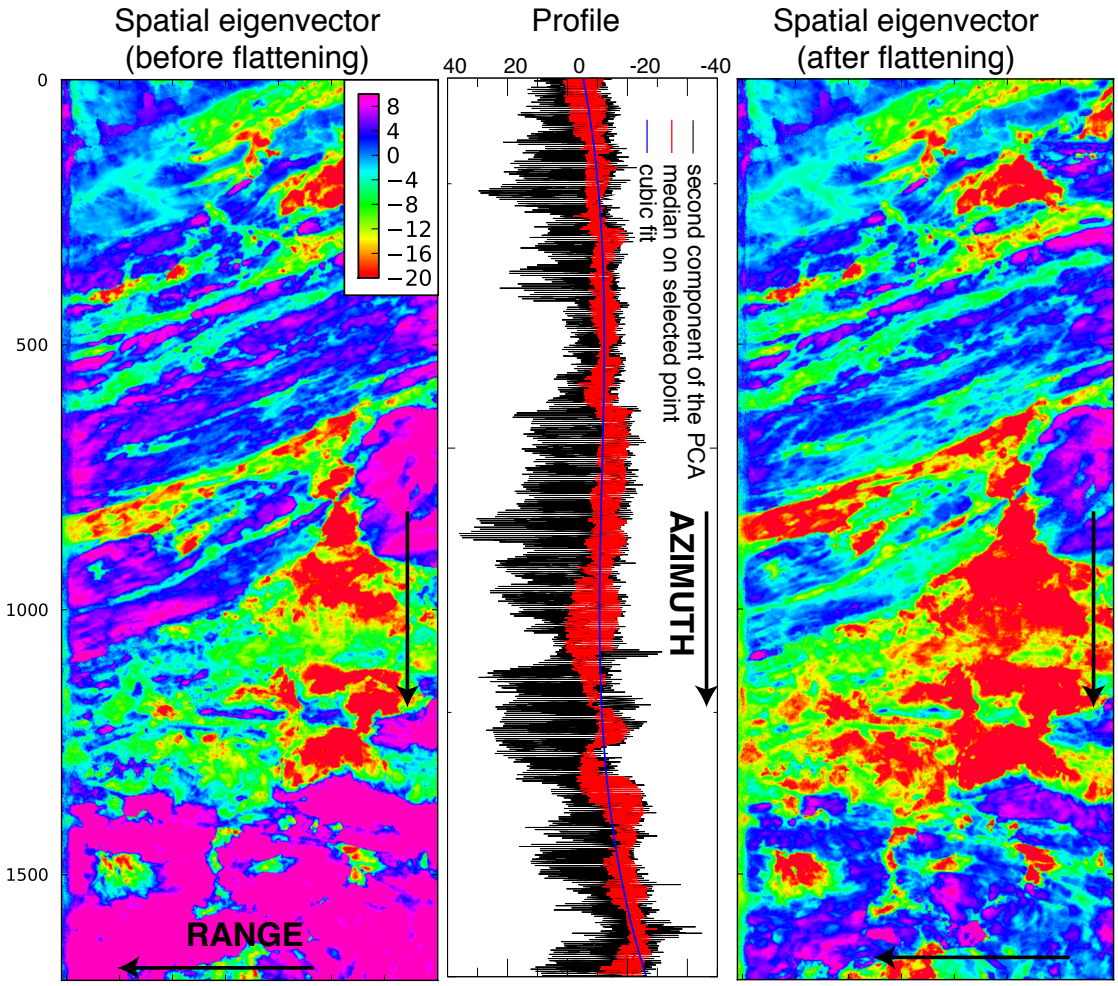

Figure S3: **Second component of the PCA decomposition for track 119.** a) Spatial eigenvector. b) Eigenvector profile (black lines). The bedrock is characterized by relatively more positive values than the basins that show more scatter. Cubic ramp (blue line) estimated from the median computed on selected points on "bedrock" (red line). c) Spatial eigenvector after flattening from the cubic ramp.

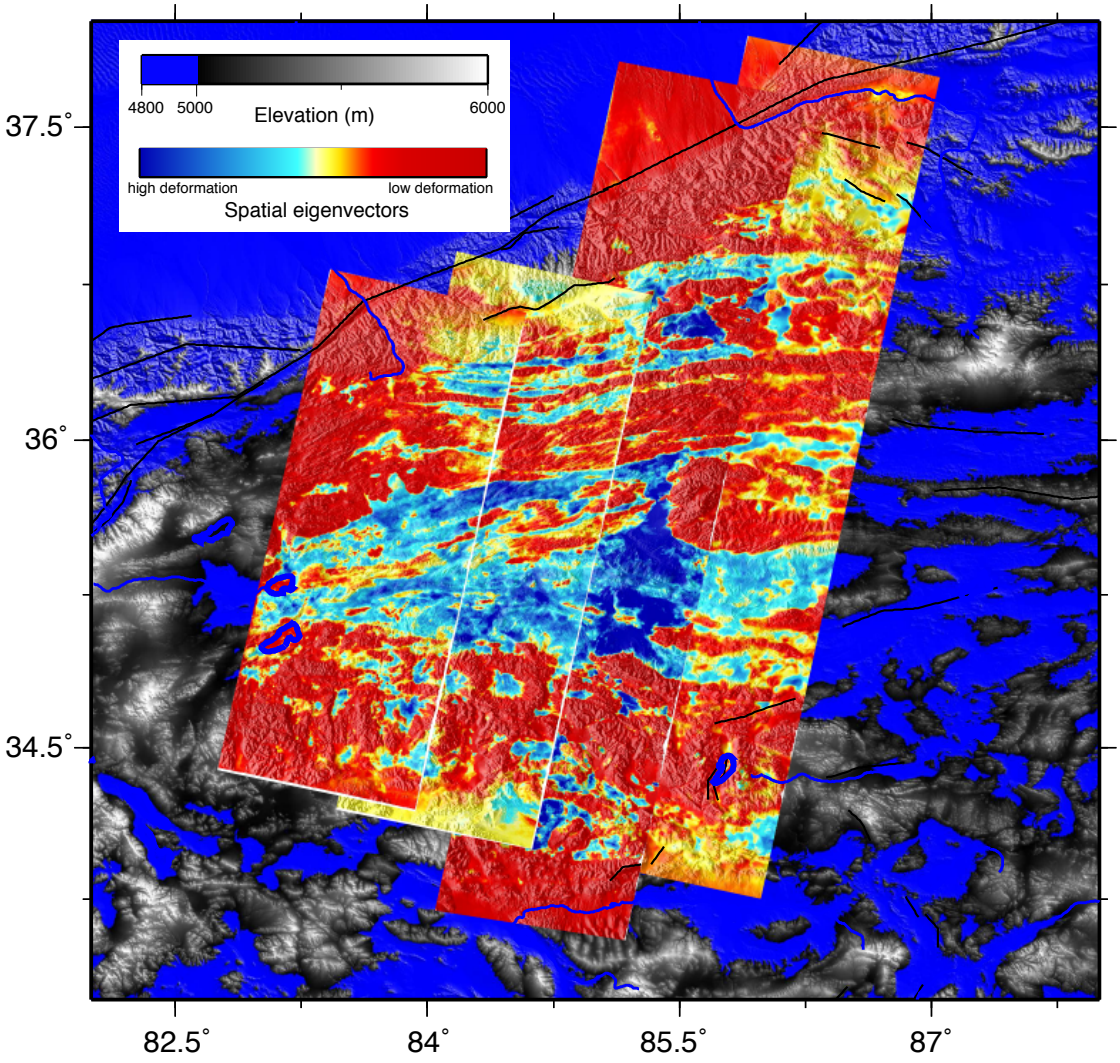

Figure S4: **Spatial eigenvectors associated to the PCA component that presents a strong seasonality.** Blue patterns are deformation areas while red colors highlight stable areas.

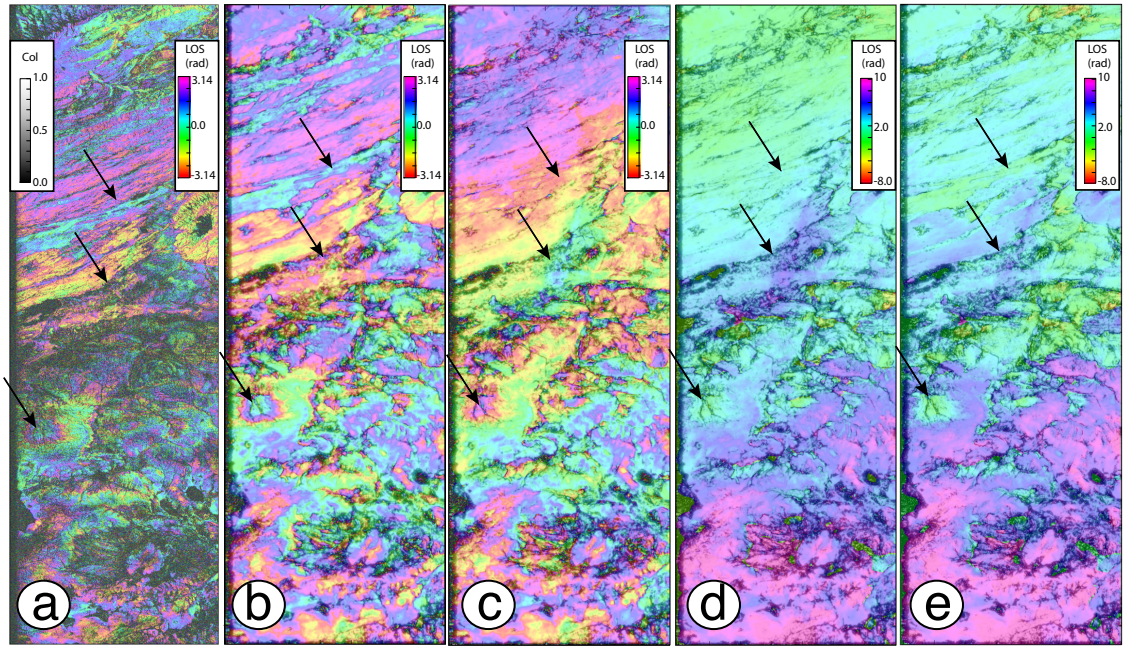

Figure S5: **Example of unwrapping procedure for an interferogram of track 119.** The interferogram is formed between the two images acquired on November 11, 2007 and April 30, 2008, for the track 119. Arrows highlight some areas with strong phase discontinuities. a) Interferogram in 8x40 looks superimposed to the phase colinearity (5). b) Filtered interferogram superimposed to the coherence associated to the filter averaging process. c) Interferogram corrected using the PCA deformation template. d) Unwrapped interferogram. e) Unwrapped interferograms after re introducing the scaled PCA shape.

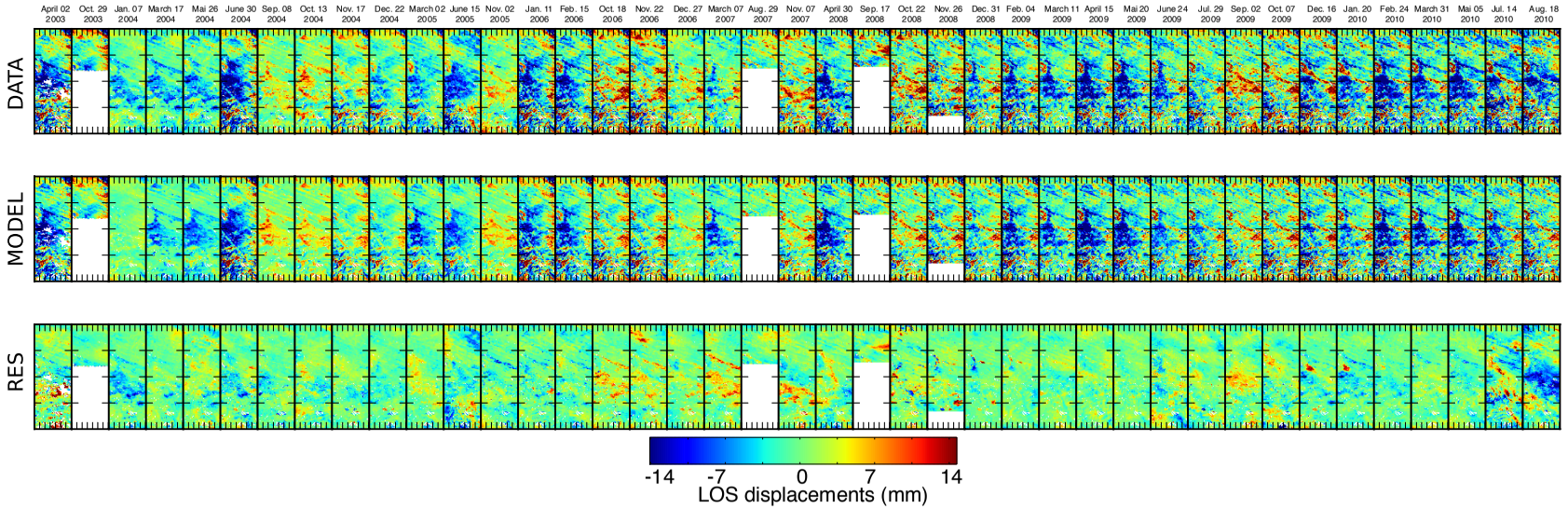

Figure S6: **Time series of delay maps, models and residuals for track 119.** One color cycle correspond to a LOS delay of 2.8 cm.